Self-consistent Models of Sagittarius A*

Scott C. Noble[(1)], Charles F. Gammie[(2,3)], Po Kin Leung[(2)]

(1) Dept. of Physics & Astronomy, Johns Hopkins University
(2) Dept. of Astronomy, University of Illinois Urbana-Champaign
(3) Dept. of Physics, University of Illinois Urbana-Champaign

Introduction:

The radio source Sagittarius A* (Sgr A*) that lies at the center of our galaxy is believed to be a hot, inhomogeneous, magnetized plasma lowing near the event horizon of a 4x106 Msun black hole. At a distance of 8 kpc the black hole is the largest black hole as judged by angular size. However, its remarkably small bolometric luminosity of

$$L \simeq 10^3 L_{sun} \simeq 10^{-8} L_{Edd}$$

provides a challenge for theoretical models. If one assumes that the accretion rate

$$\dot{M}_{X-rays} \simeq 4\mathrm{x}10^{-5} M_{sun}\, yr^{-1}$$

at r=0.1 pc based on a Bondi model and X-ray observations [1,2], holds for all r and that accretion flow is a thin disk near the black hole, then the observed luminosity is approximately

$$L \approx 10^{-5}\left(\frac{0.1}{\eta}\right) L_{thin} = 10^{-6}\left(\frac{0.1}{\eta}\right) c^2 \dot{M}_{X-rays}$$

This suggests that either the accretion rate varies with radius, the radiative efficiency is very small, the thin disk model is irrelevant, or any combination thereof. The observed spectral energy distribution (SED) disagrees with that expected from a thin disk. Recent mm and sub-mm polarimetry observations folded through a model of the accretion flow require

$$\dot{M} \sim 10^{-7} - 10^{-9} M_{sun}\, yr^{-1}$$

near the hole [3,4]. All this suggests that the accretion rate diminishes drastically as r0 .

Further, recent VLBI measurements indicate that the SED peaks near 1mm at which point emission is optically thin to within ~20 rg [5]. Hence, the properties of matter near the black hole must be well understood to make useful predictions of future mm/sub-mm VLBI observations that hope to resolve the event horizon scale. Our aim is to create self-consistent models of the optically thin emission from dynamical general relativistic magnetohydrodynamic (GRMHD) numerical simulations of the accretion flow.

GRMHD Simulations:

Since the matter surrounding the black hole is optically thin down to the horizon the innermost regions of the accretion is expected to dominate the emission. Assuming $T_e = T_{ion}$ and ideal MHD, we may presume to use the steady-state flows calculated from ideal GRMHD disk simulations such as those given in [6,7]. We use the GRMHD code called HARM, which is now publicly available from http://rainman.astro.uiuc.edu/codelib/ [8,9]. Evolutions are axisymmetric, use 256x256 cells, and involve black hole spins a = 0, 0.5, 0.75, 0.88, 0.94, 0.97. The initial conditions consist of a torus in equilibrium threaded by a poloidal magnetic field that follows density contours. The magnetic rotational instability (MRI) gives rise to a quasi-steady accreting disk. Since optically thin emission is of primary interest and cooling times are long compared to dynamical times, our omission of radiation forces from the simulation is justified.

a_* (M)	$\dot{M}_{4\mathrm{Jy}}$ $(10^{-9}\,\mathrm{M_\odot yr^{-1}})$	$\langle\dot{M}\rangle$	$\langle\dot{E}\rangle/\langle\dot{M}\rangle$	$\langle\dot{L}\rangle/\langle\dot{M}\rangle$
0.0	7.34	0.88	0.95	3.01
0.5	3.60	0.75	0.94	2.58
0.75	2.05	0.41	0.90	2.15
0.88	1.15	0.30	0.89	1.96
0.94	0.82	0.23	0.86	1.62
0.97	1.23	0.33	0.86	1.65

Table 1: Table of black hole spins used in GRMHD simulations and the corresponding values of accretion rate needed to fit observed flux density at 1mm. Also given are the energy and angular momentum accretion rates.

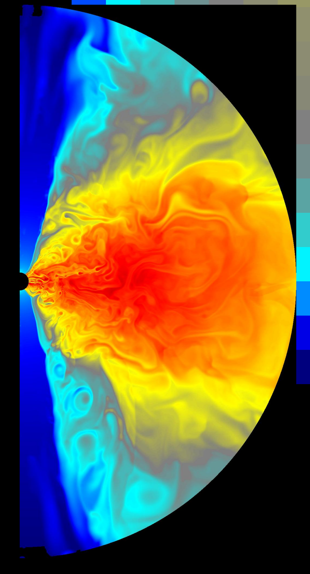

Figure 1: Log of rest-mass density from a=0.94 run.

GR Ray-Tracing:

In the ray-tracing calculations we consider non-polarized, optically thin emission from a thermal distribution of electrons. Scattering is expected to be insignificant at frequencies from 1GHz-10THz, so we neglect it. We include both synchrotron and bremsstrahlung radiation, confirming that the former dominates. Even though much of the disk is calculated to be optically thin for frequencies of interest here, there are small regions where absorption is important. For this reason, our calculations include absorption and the radiative transfer equation is solved. Rays are calculated along geodesics in Kerr backward in time from the "camera" through the simulation domain. The transfer equations are solved starting at the "end" of the geodesics and integrated back to the camera.

$$\frac{dx^\mu}{d\lambda} = N^\mu \qquad \frac{dN_\mu}{d\lambda} = \Gamma^{\nu}_{\ \mu\eta} N_\nu N^\eta \qquad \frac{d}{d\lambda}\left(I_\nu \nu^{-3}\right) = \nu^{-2}\left(j_\nu - \alpha_\nu I_\nu\right)$$

Here, x^μ is the geodesic path, N^μ is the ray's 4-velocity, j_ν is the emissivity, α_ν is the absorption coefficient, I_ν is the specific intensity.

Since one was lacking from the literature, we developed a more efficient and accurate scheme for calculating the angle-dependent synchrotron emissivity over the vast ranges in temperature and frequency found in our models. Please see [10] for details.

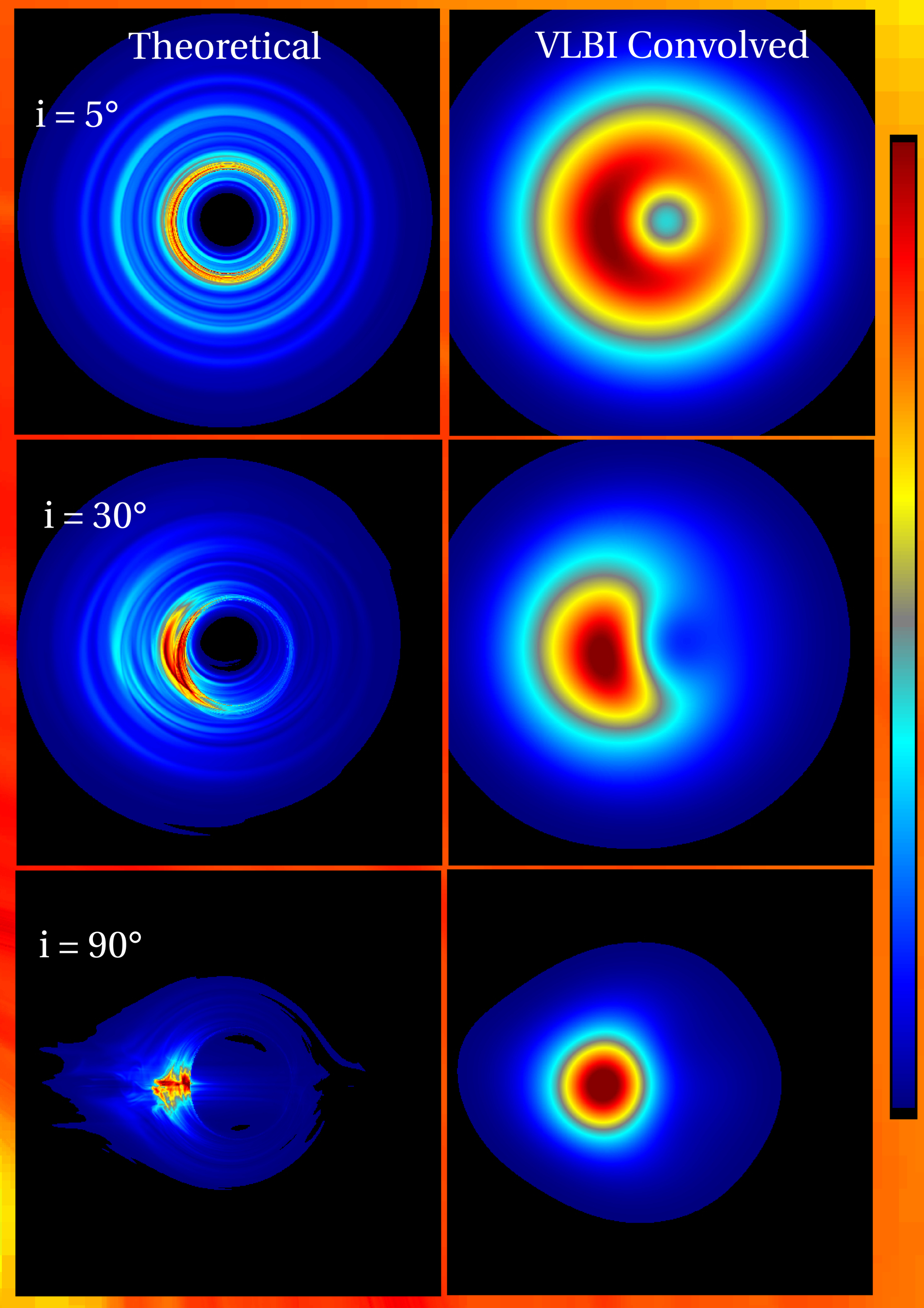

Figure 2: Ray-traced images taken at 1mm from a time slice of the a=0.94 run. Convolved images were made assuming a Gaussian beam to simulate future VLBI observations made with a 8000km baseline. Note the strong effects from relativistic beaming. At large inclinations, the hole's silhouette would not be apparent with VLBI due to this strong beaming.

Figure 3: Spectra from the ray-tracing code. Left: single time slices from runs with different black hole spin were imaged at i_{inc}=30°. Center: a single slice from the a=0.94 run were imaged at different i_{inc}. Right: different time slices from the a=0.94 run were imaged at i_{inc}=30°. For these values, we find that our model can exhibit significant variability, especially at higher frequencies. Also, we see that our model is sensitive to the spacetime and the orientation of the disk w.r.t. the observer.

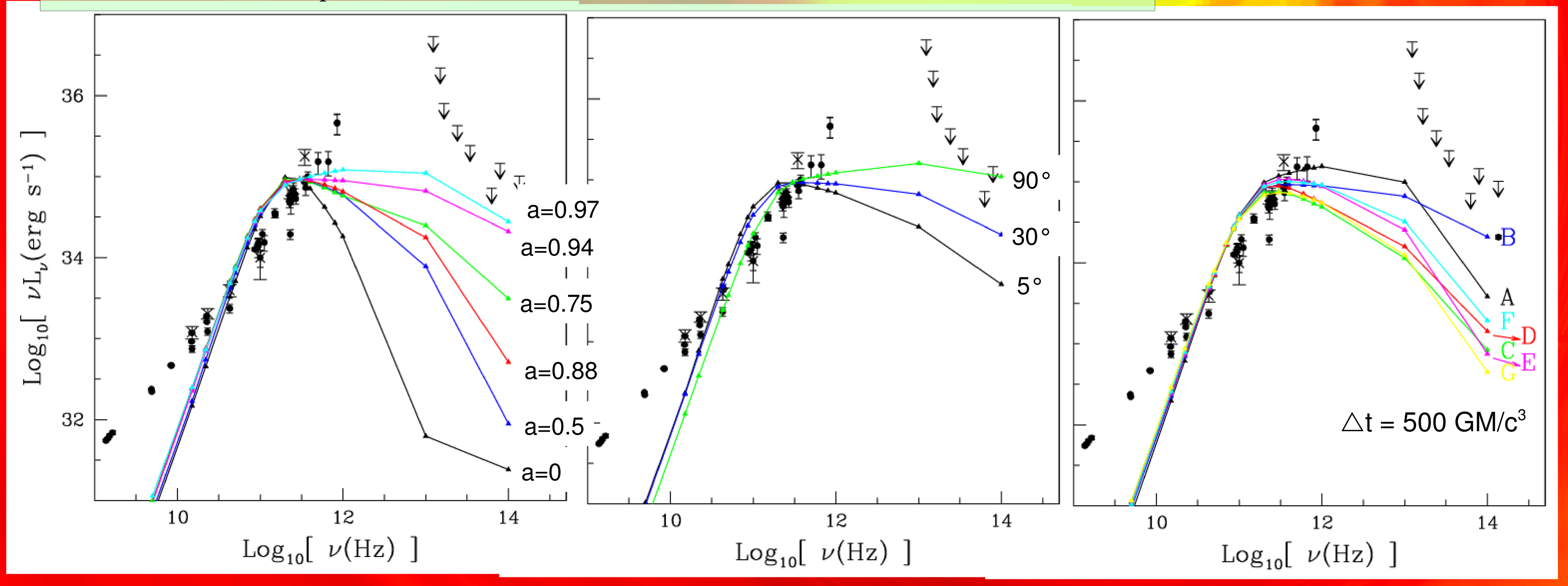

Image Refinement:

Caustics are well known to arise near strong gravitational sources [11] and our model includes turbulent structures that are small compared to the lensing object, so we expect to see significant detail in the images. They will also vary in position over time as the plasma evolves. For the ray-tracer to be successful, the intensity of a pixel's ray needs to be a good approximation of the average intensity of all light that would theoretically land on that pixel. In other words,

$$I_{ray} A_{pixel} \approx \int_{A_{pixel}} I_\nu \, dA$$

In order to uphold this approximation, we are developing an adaptive refinement algorithm to refine pixels when the LHS and RHS disagree by some adjustable amount. Since only a few percent accuracy is needed to match observational limits, we need not put stringent limits on this quantity. Our procedure consequently only performs refinement in the brightest regions.

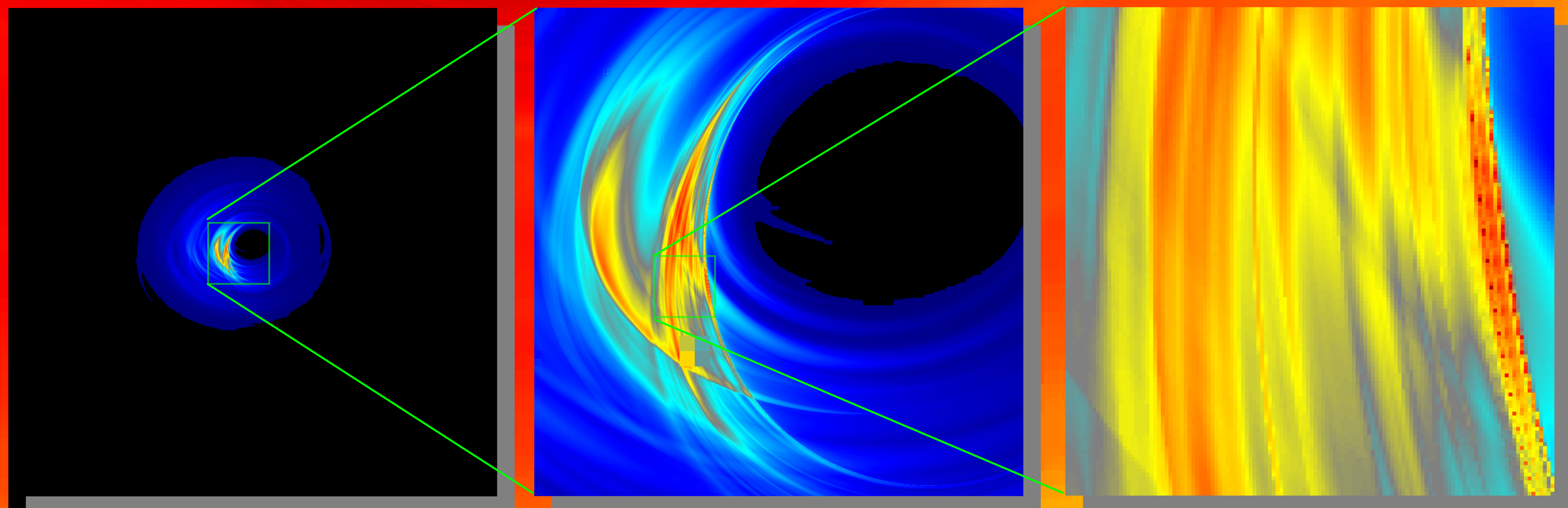

Figure 4: Left to right: segments taken from a single image with an effective resolution of 8192x8192 pixels made with the adaptive refinement procedure. The run was allowed to use up to 6 levels of refinement, with 4 child pixels per parent (bisection per dimension).

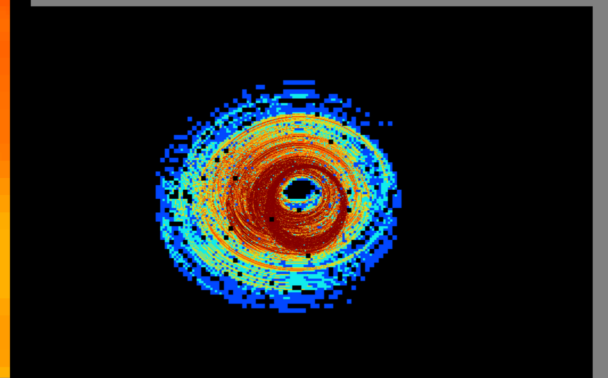

Figure 5: Left: a representation of the levels of refinement (e.g. black = 1, dark blue=2,..., dark red = 6) used in the image shown above-left.

GR Monte Carlo :

In order to investigate X-ray emission, the ray-tracing method must be abandoned for a Monte Carlo scheme that can properly calculate inverse Compton scattering, which is responsible for up-scattering synchrotron light to higher energies. Photon packets are emitted with particular angle and frequency dictated by the thermal synchrotron emissivity function [12]. The packets are propagated until its optical depth has reached ~10 or it reaches a specified collecting radius far from the disk.

Figure 6: Paths of photons emitted isotropically in the frame of a fluid element near the black hole using the MC code.

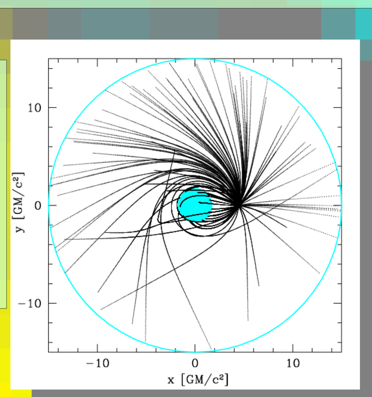

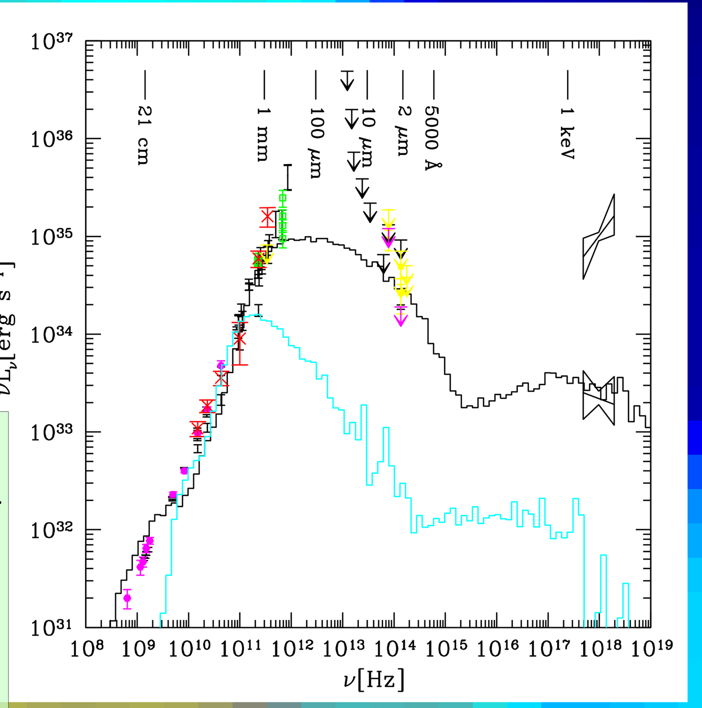

Figure 7: MC spectra including Compton scattering calculated from a time slice of the a=0.94 run. Black line is the SED collected near i_{inc} = 90º, and the cyan line is that for i_{inc} = 0º. Observations are overlaid, with down-pointing arrows indicating upper limits. Note that the spectrum at i_{inc} = 90º agrees with all portions of the spectrum, including the quiescent X-ray emission.

Figure 8: Distribution of the average radius of emission for a=0.94. Black curve corresponds to i_{inc} = 90º, and the cyan curve to i_{inc} = 0º. Note the non-trival function of frequency and the fact that most emission originates near the horizon.

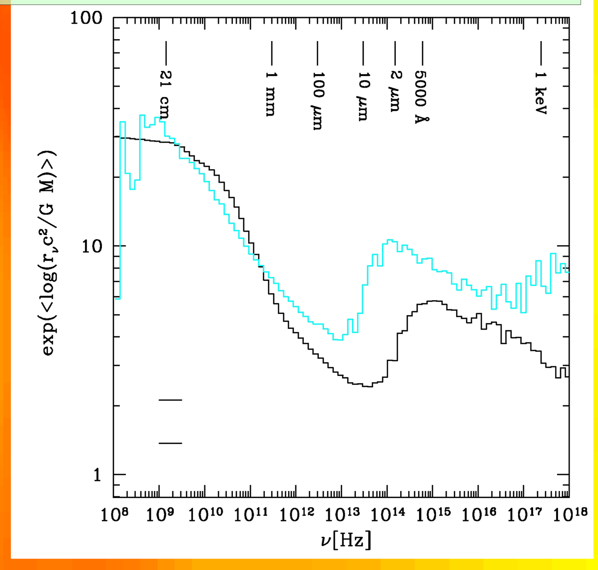

Figure 9: Average change in azimuth from emission to observation for a=0.94. Black curve corresponds to i_{inc} = 90º, and the cyan curve to i_{inc} = 0º. The horizontal black line indicates emission from an isotropic distribution of plasma surrounding the black hole. At high frequences and inclinations, it is common for most of the emission to orbit the hole at least once.

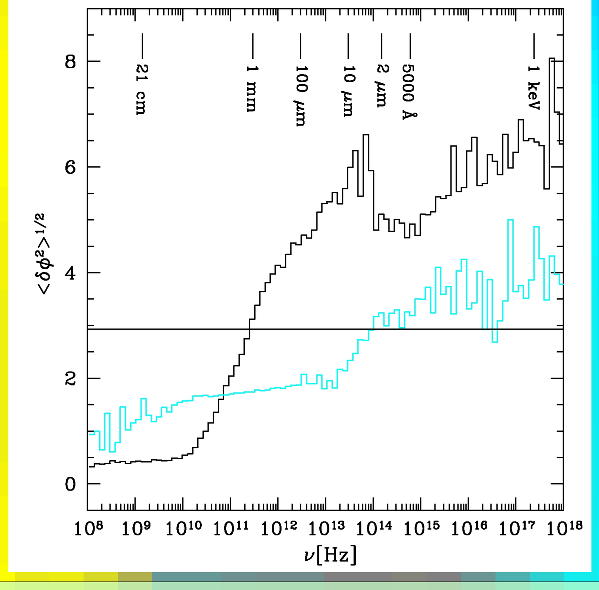

Summary:

- Relativistic effects are important.
- Spectra are sensitive to inclination and black hole spin.
- Average emission radii have non-trivial frequency-dependence.
- Emission sensitive to disk inhomogeneities and evolution.
- Silhouette observable for i < 30º at 1mm w/ 8000km VLBI baseline.

Future work:

- Include polarization to measure Faraday rotation.
- Perform timing analysis (image shape, spectra, polarization...)
- Use 3D simulation data.

Bibliography:

[1] F. K. Baganoff et al., ***Nature***, **413**, 45 (2001).
[2] F. K. Baganoff et al., ***ApJ***, **591**, 891 (2003).
[3] J. P. Macquart et al., ***ApJL***, **646**, L111 (2006).
[4] D. P. Marrone et al., ***arXiv:astro-ph/0607432***.
[5] Z. Q. Shen et al. ***Nature***, **438**, 62 (2005).
[6] J. C. McKinney & C. F. Gammie, ***ApJ***, **611**, 977 (2004).
[7] S. C. Noble et al., *accepted* to **CQG**, ***arXiv:astro-ph/0701778***.
[8] C. F. Gammie et al., ***ApJ***, **589**, 444 (2003).
[9] S. C. Noble et al., ***ApJ***, **641**, 626 (2006).
[10] P. K. Leung, S. C. Noble, C. F. Gammie, *to be sub.* ***ApJS*** (2007).
[11] K. P. Rauch & R. D. Blandford, ***ApJ***, **421**, 46 (1994).
[12] C. F. Gammie, S. C. Noble, P. K. Leung, *to be sub.* ***ApJ*** (2007).

Acknowledgments:

We thank Laura Book for an early version of the ray-tracing code. This research was supported by NSF grants AST 00-93091 and PHY 02-05155.